Mechatronic Considerations for Actuation of Human Assistive Wearable Robotics: Robust Control of a Series Elastic Actuator

Kyoungchul Kong[1], Joonbum Bae[2], and Masayoshi Tomizuka[3]

[1] Department of Mechanical Engineering, Sogang University, Korea
[2] School of Mechanical and Advanced Materials Engineering, UNIST, Korea
[3] Department of Mechanical Engineering,
University of California, Berkeley, CA, USA

Abstract. To realize ideal force control of robots that interact with a human, a very precise actuating system with zero impedance is desired. For such applications, a rotary series elastic actuator (RSEA) has been introduced recently. This chapter presents the design of RSEA and the associated control algorithms. To generate joint torque as desired, a torsional spring is installed between a motor and a human joint, and the motor is controlled to produce a proper spring deflection for torque generation. When the desired torque is zero, the motor must follow the human joint motion, which requires that the friction and the inertia of the motor be compensated. The human joint and the body part impose the load on the RSEA. They interact with uncertain environments and their physical properties vary with time. In this chapter, the disturbance observer method is applied to make the RSEA precisely generate the desired torque under such time-varying conditions. Based on the nominal model preserved by the disturbance observer, feedback and feedforward controllers are optimally designed for the desired performance: i.e. the RSEA 1) exhibits very low impedance and 2) generates the desired torque precisely while interacting with a human. The effectiveness of the proposed design is verified by experiments.

Keywords: Rotary series elastic actuator, Disturbance observer, Force mode control, Human-robot interaction, Motor impedance.

1 Introduction

Mechatronics technologies play significant roles in applications that improve quality of life. Active assistive devices, such as motorized wheel chairs or active prosthetics, are some of examples. They have improved the mobility of many people with disabilities, which allowed them to engage their everyday lives with much less difficulties. In the last decade, power assistive devices based on mechatronic technologies are being developed in the form of wearable robots for assisting physically impaired people or for augmenting human power.

Fig. 1 shows the basic structure of an assistive robot interacting with a human. The human body ((a) in the figure) is the plant to be controlled. The

body is actuated by the muscles which are controlled by the brain. Since the desired motion is intrinsically generated in the brain by intention or reflex, the human has a fully closed control loop with no external input. If a human has either nervous or muscular disorders, or needs extra forces to perform demanding work, an assistive robot ((d) in Fig. 1) may provide additional forces (τ_A) to the human body. Recently, various assistive robots have been developed: Sankai developed HAL (Hybrid Assistive Limb) for augmenting power of normal persons [1], [2], and Kazerooni introduced BLEEX (Berkeley Lower Extremity Exoskeleton) for military applications [3], [4]. Yamamoto developed Power Assist Suit to assist nurses lifting heavy patients [5], and Kong and Jeon introduced EXPOS (Exoskeleton for Patients and Old people by Sogang University) for weakened persons [6], [7].
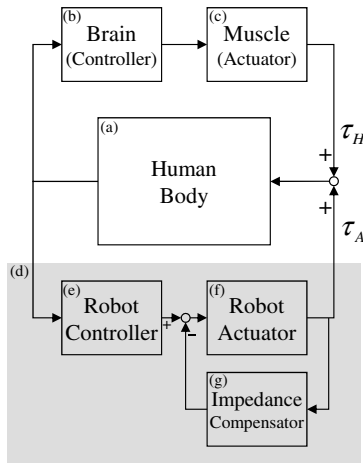

Fig. 1. Conceptual structure of an assistive robot interacting with a human

Many approaches also have been proposed for the controller ((e) in Fig. 1) and the actuator ((f) in the figure). The main role of the controller in this application is to determine the magnitude and the direction of forces for interacting with a human (e.g. assistive forces or feedback forces for rehabilitation). Since it is impossible to directly detect the human intention, the controller usually sets the references for the assistive forces based on the estimated values obtained by the biological sensors [1], [5], [7] or the dynamical properties [3], [8]. For examples, HAL applies EMG (electromyography) sensors to measure muscular efforts [1], and BLEEX calculates the required forces based on the inverse dynamics method [3]. Power Assist Suit applies a novel sensor called the muscle hardness sensor [5]. Since these methods are for estimation of human joint torques during motions, they are usually utilized for assisting healthy/intact people. In applications for patients, an impedance control method [9], [10], [29] is often used. In this case,

a motion trajectory for a patient is predefined for the purpose of rehabilitation [9], and a robot assists the patient to follow the desired motion [9]-[11].

Controllers for human-robot interaction may assume that actuators are operated in an ideal force (or torque) mode control. The ideal force mode implies: 1) the actuator has (output shaft) zero impedance so that it is perfectly backdrivable, and 2) the force (torque) output is exactly proportional to the control input. Researchers have tried to find such actuators for human-robot interaction. For examples, HAL applies DC motors [1], [2], and BLEEX utilizes hydraulic actuators [4]. Power Assist Suit uses pneumatic actuators [5]. EAP (Electroactive Polymer) and rubber-muscle actuators also have been developed recently [12], [13]. In spite of these efforts, lack of a suitable actuator is still evident in the applications involving human-robot interaction. Recently, progresses have been made to overcome the problems encountered in actuators such as friction and rotor inertia by applying an algorithmic compensator [see (g) in Fig. 1]. For example, Buerger and Hogan introduced the complimentary stability and loop shaping method to design the compensator computationally [14]. From the viewpoint of hardware as well as controller designs, series elastic actuators are noteworthy [15]-[21]. In these cases, a spring is installed between an actuator and a human joint and plays the role of an energy buffer as well as a force sensor. The force is generated from the differential position or the deflection of the spring, which is controlled by a position controller [15], [16]. This implies that the impedance compensator in Fig. 1 is accomplished based on a position control method. The spring isolates the human joint from undesired factors of the motor including rotor inertia and nonlinearities. However, it also introduces challenges to the design of a control algorithm. For example, mechanical compliance in the actuation does not offer only advantages without costs. Also, the lower the stiffness, the lower the frequency with which larger output forces can be modulated. Due to the interaction with a human, dynamic characteristics of the whole system is time varying. Therefore, the performance of such actuators is determined by how the control algorithm robustly controls the spring deflection under the time-varying conditions. Namely, the controller of actuators for human-robot interaction should meet the following performance objectives:

1. it reduces mechanical impedance of the actuator by compensating for the inertia and the friction of the actuator,
2. it makes the actuator precisely generate the torque as desired, and
3. it guarantees the robust performance of the actuator while interacting with a human.

In this chapter, the design of controllers for a rotary series elastic actuator (RSEA) is discussed. To assure the robust performance of the RSEA, a disturbance observer is utilized as well as the feedback and feedforward controllers.

This chapter is organized as follows. The basic properties and problems of a geared motor are reviewed in section 2. Hardware design of a RSEA is discussed in section 3. In section 4, a robust control algorithm for the RSEA is designed and its properties are analyzed. The designed control algorithm is evaluated by experiments in section 5. Summary and conclusions are given in section 6.

2   Open Loop Torque Mode Control of Geared DC Motor

Motors have been widely used in applications involving human-robot interaction due to their superior controllability and flexibility. The capacity of a motor is defined by the maximum allowable power, i.e. a multiplication of the angular velocity and the generated torque. Since a motor has physical limitations on the maximum velocity and the maximum torque, the operation range is adjusted by a reduction ratio. The use of reducers introduces various nonlinearities such as friction and backlash. The generated torque is magnified by the reduction ratio, but the rotor inertia and the friction force are also amplified significantly.

Motor impedance, or mechanical impedance, represents a measure of how much the motor resists motion when subjected to a given force. Mathematically, it is defined as the ratio of the force applied to the mechanical system to the resulting velocity of the system, i.e.

$$Z(\omega) = \frac{f(\omega)}{v(\omega)} \tag{1}$$

where $Z(\omega)$ is the motor impedance, $f(\omega)$ is the resistive force, and $v(\omega)$ is the velocity. $f(\omega)$ consists of the following terms:

$$f(\omega) = f_{friction}(\omega) + f_{damping}(\omega) + f_{inertia}(\omega) + f_{bias}(\omega) + \Delta f(\omega) \tag{2}$$

where $f_{friction}(\omega)$ is the coulomb friction force which increases the motor impedance in the low frequency range. $f_{damping}(\omega)$ represents the linear damping force and increases the motor impedance over the entire frequency range. $f_{inertia}(\omega)$ is resulted from Newton's second law, and increases the impedance in the high frequency range. $f_{bias}(\omega)$ is the bias value of force output and $\Delta f(\omega)$ represents forces due to other factors.
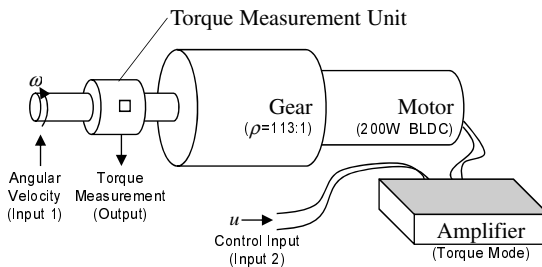

Fig. 2. Experimental setup for motor impedance test

For most dynamic systems such as industrial robots and machining tools, the mechanical impedance of an actuator should be sufficiently large for a large frequency bandwidth and effective rejection of disturbances [22]. For example, an actuator for a machine tool must be insensitive to any applied disturbance forces
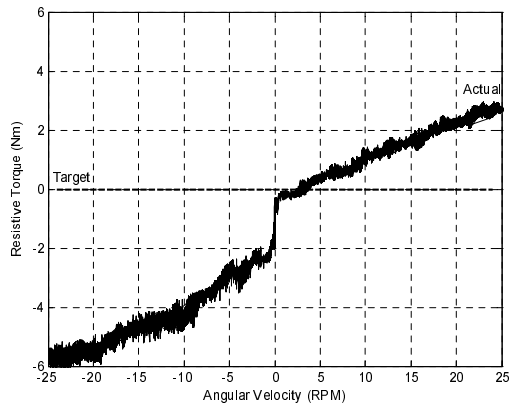
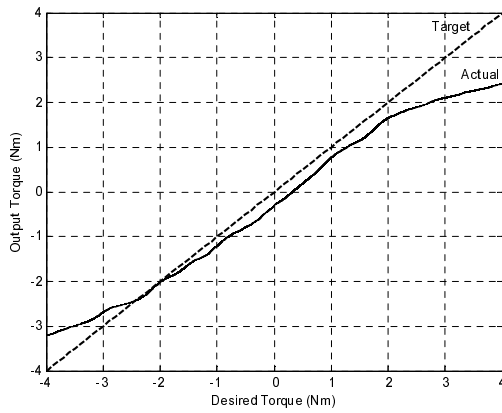**Fig. 3.** Motor impedance test: the control input is fixed to zero

Fig. 4. Linearity test: the angular velocity is fixed to zero

for the best quality of products. However, this paradigm is no longer applied to applications interacting with a human. The most important factor of actuators in such applications may be the comfort of a human, i.e. the actuator should not resist the human motion and generate only the desired force. In other words, the actuators for human-robot interaction must have low mechanical impedance [9], [14]. This requirement creates challenges to the selection of actuators. To realize the ideal actuator, every term in (2) should be eliminated. Also, the large frequency bandwidth is no longer an issue as long as they have the bandwidth up to the frequency range of human motions which is about $4 \sim 8 Hz$.

Fig. 2 shows an experimental setup for testing the mechanical impedance of a DC motor. The output torque was measured by a torsional spring. The detailed information on the spring used in this chapter will be discussed in section 3. Ideally, the torque sensor in Fig. 2 should read zero regardless of the angular velocity when the control input is zero [see Target line in Fig. 3]. However, due to the friction force and the rotor inertia of the actual device, the torque sensor reads the resistive torque in actual experiments [see Actual line in Fig. 3]. The experiment in Fig. 3 was performed for testing the relationship between the resistive torque and the angular velocity while the control input is zero. Note that the magnitude of the bias force was so large that the motor rotates even with zero input. This phenomenon often occurs in the applications of DC motors. This problem can be solved by fine tuning the amplifier. However, the default setting was used in the experiment to test in normal conditions. The discontinuity at $\omega = 0$ represents the static friction force. In addition, the motor has nonlinearities related to the control input. Fig. 4 shows the result of the linearity test about the control input u when the rotor was fixed mechanically (i.e. $\omega = 0$). To observe the linearity excluding the static friction effects, the curve in Fig. 4 was obtained by taking the average of many experimental data. In the ideal case, the curve in Fig. 4 should be a straight line which passes through the origin [see Target line in the figure]. However, the actual profile obtained is a nonlinear curve which does not pass through the origin [see Actual line in the figure]. The undesired characteristics (i.e., the damping, Coulomb friction, and input-output nonlinearity) discussed with Figs. 3 and 4 should be eliminated to realize the ideal human-robot interaction.

3   Rotary Series Elastic Actuator

3.1   Hardware Configuration

An actuator interacting with a human may be a burden to the human body because of its mass and friction. For ideal human -robot interaction, the actuator should be controlled in the force (or torque) mode [9], [10], [17], [19]. In reality, however, most actuation systems do not generate the desired torque precisely as discussed in the previous section. Another problem occurs when the desired force is less than the friction of the actuator.
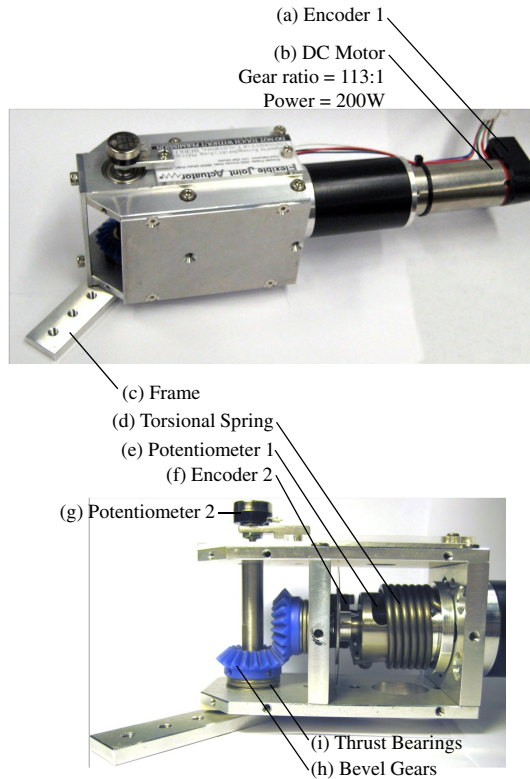
(a) Encoder 1

(b) DC Motor
Gear ratio = 113:1
Power = 200W

(c) Frame
(d) Torsional Spring
(e) Potentiometer 1
(f) Encoder 2
(g) Potentiometer 2

(i) Thrust Bearings
(h) Bevel Gears

Fig. 5. Rotary series elastic actuator

To compensate for the resistive forces, force sensors such as a loadcell and a strain-gauge are often installed at the load side of a rigid reducer [23], [24]. The motor is feedback controlled by the force measurements. This method has shown good performances in industrial applications involving force mode actuation [23], [24]. However, it is not suitable for the applications of human-robot interaction, since the rigidity of the reducer may cause discomfort or even damage to the user. For such applications, it may be better to have compliance in the reducer such that a human does not feel the resistance when he/she initiates motions.

A solution to this problem is to utilize a mechanism which may serve as a buffer between the actuator and the human joint. For example, in power management of an automobile a clutch mechanism serves as the buffer to connect the engine and varying load due to vehicle motion and environment. Similarly, in actuators of robots interacting with human, a spring serves as the buffer. The actuator is controlled such that the spring between a human joint and the actuator has proper deflection. Now we have two sub-systems: the human body and the actuation system, where the mechanical power for interacting with the human is transferred through a spring.

An actuating system with a torsional spring is called a rotary series elastic actuator (RSEA). The similar approach is shown in [15], [17]-[21] where it applies a linear spring for the same purpose. If the linear spring is used, the structure of the actuator system is similar to that of a muscle. However, it requires torque arms for generating the joint torque. In the design of RSEA, a torsional spring is directly installed between a human joint and a motor such that it can generate the joint torque uniformly over the entire angular range. A RSEA consists of a DC motor, a spring and two encoders as shown in Fig. 5. The position of the DC motor is controlled to have the desired spring deflection such that the RSEA generates the desired torque precisely. Since the human joint angle is required to determine the desired spring deflection or the reference position of the motor, an additional encoder ((f) in Fig. 5) is installed. The joint angle is limited by the angle limiter to protect the patient in case of a malfunction. The overall design is shown in Fig. 5.

3.2 Spring Selection

Since the spring is utilized as a torque sensor as well as a torque generator, the performance of RSEA depends on characteristics of the spring. For example, the maximum torque of RSEA is determined by stiffness of the spring. If the spring is too stiff, however, a human may feel discomfort. Therefore, the spring should be optimally designed considering both the maximum torque and the control performance of the motor.
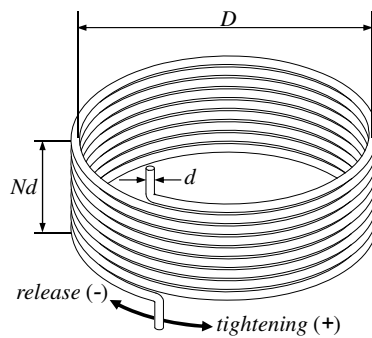

Fig. 6. Design of a torsional spring

Fig. 6 shows the mechanical design of a torsional spring installed in the RSEA ((d) in Fig. 5). The spring constant is determined by D, d, N in Fig. 6 and the elastic modulus of the material [25]. The specific parameters are shown in Table. 1. The desired maximum deflection was determined by considering the encoder resolutions.

Table 1. Specification of a torsional spring

Specification	Values
Encoder resolution of motor side	56500 counts/rev. (encoder resolution: 500 counts/rev. gear ratio: 113:1)
Encoder resolution of human side	2000 counts/rev.
Desired maximum deflection	±25 degrees
Desired maximum torque	±6 Nm
Mean diameter of spring D	33 mm
Wire diameter d	5 mm
Number of turns N	6
Measured spring constant k	0.32 Nm/deg
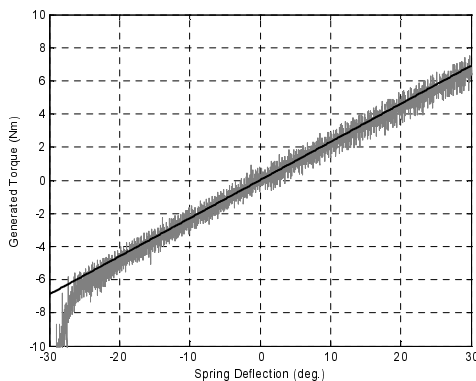
Fig. 7. Experimental result of deflection angle of the spring and generated torque

In general, a spring is a nonlinear element: i.e. the spring force is a nonlinear function of the spring deflection. Since the generated torque is estimated by the spring deflection in this application, the nonlinearity may affect the control performance, i.e. the generated force may be different from the estimated torque. To check the nonlinearity of the spring, an experiment was performed. The body of RSEA was fixed on the ground such that the frame ((c) in Fig. 5) presses a loadcell for measurement of the generated force. The force is converted into the torque by multiplying the torque arm, i.e. the length of the frame. Fig. 7 shows the experimental results of the relation between the spring deflection and the measured torque. It is desired that the curve is a straight line that passes through the origin. As shown in the figure, the spring used in the experiment shows very good linearity in the desired deflection range. The stiffness blows up at a certain deflection angle [see -25 degrees in the figure] because the spring is mechanically constrained. Since the relation shown in the figure is close to linear in the desired deflection range, the spring is regarded as a linear element in this chapter.

4   Controller Design for Rotary Series Elastic Actuator

4.1   System Modeling

A RSEA installed on a human joint is depicted in Fig. 8, where I_H and C_H are the inertia and the damping coefficient of human joint, and I_M and C_M are those of the geared motor, respectively. Since I_H and C_H are different from person to person and from segment to segment, they are treated as unknown parameters in this chapter. The motor and the human joint are connected via a torsional spring with spring constant k. τ_H and τ_M represent the human muscular torque and the motor torque, and θ_H and θ_M are the angle of the human joint from the neutral position and that of the motor respectively. The neutral position of a human body segment is not necessarily the vertical axis (e.g. feet). A RSEA can be modeled as a multi-input and multi-output system where inputs are the actuator torque and the muscular torque, and outputs are the actuator angle and the human joint angle. The controlled output is the spring torque which is proportional to the spring deflection, i.e. the difference between the actuator and the human joint angle.
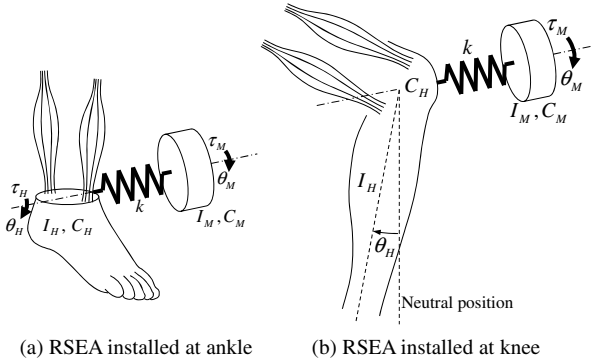

(a) RSEA installed at ankle   (b) RSEA installed at knee

Fig. 8. Schematic plots of human joints and rotary series elastic actuators

By Hooke's law, the torque output, τ_A, of the RSEA is

$$\tau_A = k(\theta_M - \theta_H) \tag{3}$$

Subscript A denotes that the quantity represents the assistive torque to human. Based on (3), the desired position of the motor is expressed as a function of the desired torque, i.e.

$$\theta_{M,Desired} = \theta_H + \frac{\tau_{A,Desired}}{k} \tag{4}$$

Note that if the motor tracks the desired position exactly, i.e., $\theta_M = \theta_{M,Desired}$, then the RSEA exactly generates the desired torque rejecting every undesired factor such as friction. Therefore, a precision control algorithm may improve the

performance of RSEA. In (3) and (4), the spring is assumed to be linear. In the case of a nonlinear spring, the inverse of the describing function should be used in (4) instead of the use of the inverse of the spring constant.

The governing equation for the system in Fig. 8 is

$$\begin{bmatrix} I_M & 0 \\ 0 & I_H \end{bmatrix} \ddot{\Theta} + \begin{bmatrix} C_M & 0 \\ 0 & C_H \end{bmatrix} \dot{\Theta} + \begin{bmatrix} k & -k \\ -k & k \end{bmatrix} \Theta = \begin{bmatrix} \tau_M \\ \tau_H - mgl\sin(\theta_H) \end{bmatrix} \quad (5)$$

where, Θ is $[\theta_M \ \theta_H]^T$, m is the mass of human body segment, g is the gravity constant, and l is the distance between joint and center of mass of body segment. The dynamic equation assumes that there is no constraint imposed on either the motor or the human joint. However, the joint is subjected to constraints during some motion phases. For example, if the foot is touching the ground, it may be reasonable to assume that the human side of the spring is grounded as shown in Fig. 9(b). In this case, (5) no longer applies. Thus the human joint actuation system requires multiple dynamic models for complete description of its dynamic behavior. A possible approach to handle such a system is the discrete event system approach. In this chapter, we explore an approach to design a controller for a nominal model. Actual dynamics is regarded as perturbed dynamics.

Assume that there is a relation between the motor angle and the spring deflection, i.e.

$$\frac{E(s)}{\theta_M(s)} = \alpha(s) \quad (6)$$

where $E(s) = [\theta_M(s) - \theta_H(s)]$. $\alpha(s)$ is obtained by setting $\tau_H = 0$ in (5) which assumes that the human force is an external disturbance, i.e.

$$\alpha(s) = \frac{I_H s^2 + C_H s + mgl}{I_H s^2 + C_H s + k + mgl} \quad (7)$$

where $\sin(\theta)$ has been approximated by θ for simple analysis. If τ_H controls the human joint motion, the inertia that the motor sees, I_H, is increased significantly. If actual external forces are imposed on the human body (e.g. ground contact forces in feet), the effective inertia is also increased. In these cases, I_H in (7) is not the pure inertia of the human body segment, but the effective inertia imposed on the RSEA. Namely, $\alpha(s)$ is a transfer function resulted from human-robot interaction which is unknown and time-varying. By multiplying the spring constant k on both sides of (6), the relation between the motor angle and the spring torque is obtained from (3) as

$$\tau_A(s) = kE(s) = k\alpha(s)\theta_M(s) \quad (8)$$

By Newton's third law, the spring torque is exerted to the motor system as well as the human body. Therefore, the dynamics of the motor part is

$$I_M \ddot{\Theta}_M + C_M \dot{\Theta}_M = \tau_M(t) - \tau_A(t) \quad (9)$$

Combining (8) and (9), a transfer function from τ_M to θ_M is obtained as

$$\Psi(s) = \frac{1}{I_M s^2 + C_M s + \alpha(s)k} \quad (10)$$

$\Psi(s)$ represents a possible model set of the RSEA. Note that the model is time-varying as $\alpha(s)$ changes due to human-robot interaction. Fig. 9 shows two extreme cases.

Case 1

Case 1 in Fig. 9 applies during swinging of a leg. During the swing motion of the normal gait, the movements of ankle and knee joints are large. In this case, it is a reasonable assumption that the joint motion is mainly resulted from the gravity and the assistive torque, and the transfer function from $\tau_M(s)$ to $\theta_M(s)$ is

$$P_1(s) = \frac{1}{I_M s^2 + C_M s + \alpha(s)k} \in \Psi(s) \qquad (11)$$

where $\alpha(s)$ is given by (7) and its magnitude depends on the physical properties of human body segments. In this case, I_H in $\alpha(s)$ represents the pure inertia of a human body segment.
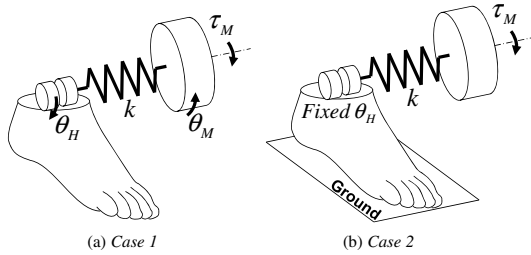

(a) *Case 1*   (b) *Case 2*

Fig. 9. Two possible cases of human joint

Case 2

During the stance phase of the normal gait and standing up motion, the movements of ankle and knee joints are slow while the required joint torque is large. Therefore, the motion of the actuator is much larger than that of the human joint. Moreover, since the body segment is grounded, a constraint is imposed on the human joint. This may be regarded as a significant increase of I_H in (7), i.e. $I_H \gg 1$, which results in $\alpha(s) \approx 1$, i.e.

$$P_2(s) = \frac{1}{I_M s^2 + C_M s + k} \in \Psi(s) \qquad (12)$$

Fig. 10 shows the frequency responses of the two cases mentioned above with reasonable physical values of the ankle joint. Since $P_2(s)$ in (12) has the minimum order in the possible model set and does not require properties of human body which are usually difficult to measure, the transfer function of (12) is used as a nominal model in this chapter.
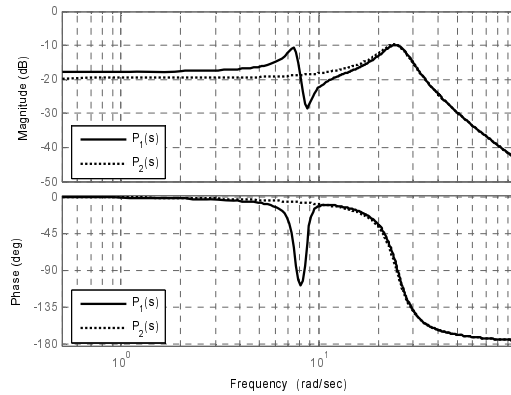
Fig. 10. Frequency responses of *Case 1* and *Case 2*: $P_1(s)$ and $P_2(s)$ are as defined by (11) and (12).

4.2   Force Feedback Control

To improve the tracking performance, a feedback control algorithm is required. For the design of the controller, the control loop is reconfigured as shown in Fig. 11. In the figure, E_D represents the desired spring deflection calculated by (3). The aim of the controller ($C(s)$ in the figure) is to maintain the desired spring deflection regardless of the variations of the system model. Since the spring deflection is directly related to the generated force (torque), the control system in Fig. 11 can be regarded as a force feedback system where the force is estimated by the spring deflection.
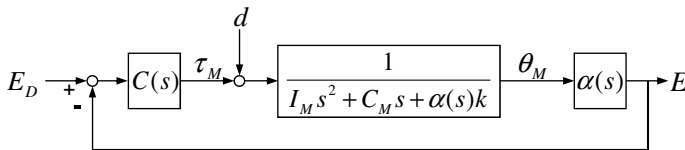

Fig. 11. Block diagram of the Joint Controller: The desired deflection E_D is obtained by (3) and d represents the exogenous disturbances.

Fig. 12 shows the location of poles and zeros of the open loop transfer function from τ_M to E in Fig. 11. By increasing I_H in $\alpha(s)$, poles and zeros converge to the points labeled (d) in Fig. 12. Note that there is a weakly damped complex pole-zero pair and the pair moves towards the imaginary axis as I_H is increased. As I_H approaches infinity, they asymptotically cancel each other, and the open loop transfer function is asymptotic to (12).

A simple and effective controller is a PD (Proportional- Derivative) controller. If the zero of the PD controller is fixed, the closed loop poles shift as shown in
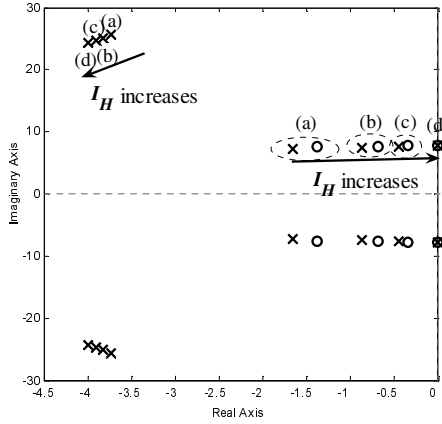
Fig. 12. Poles and zeros of the open loop transfer function: (a), (b), (c) and (d) apply for the ankle joint of the $50\%^{ile}$ female, the knee joint of the $50\%^{ile}$ female, the knee joint of the $50\%^{ile}$ male and the constrained joint respectively.

Table 2. Properties of human body segments used in Fig. 12 [26]

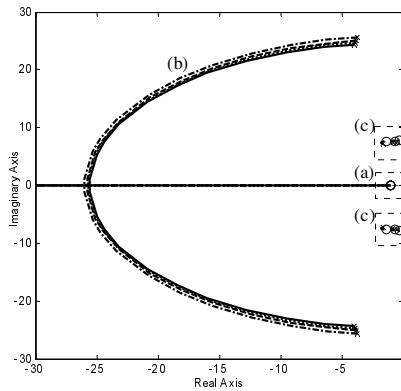| Human Body Segment	Moment of Inertia I_H (kgm^2)
Foot of the $50\%^{ile}$ female	0.027
Foot and shank of the $50\%^{ile}$ female	0.459
Foot and shank of the $50\%^{ile}$ male	0.660

Fig. 13. Root loci applying the PD controller: Arrows indicate increasing control gains for a fixed P-D gain ratio

Fig. 13 for the varying control gain from 0 to ∞. As the gain of the PD controller is increased from zero, the closed loop poles on the branch (b) in Fig. 13 move away from the imaginary axis and move toward the real axis which means that the response becomes faster and less vibratory. If the gain is excessively large, a real pole moving toward the origin will slow down the response speed. As mentioned already, the open loop poles and zeros defining branch (c) in Fig. 13 are very close to each other, and they minimally influence the closed loop transfer function.

More quantitative way to tune the PD control gains is to apply the LQ (Linear Quadratic) method. The LQ method is applicable when the nominal model in (12) is expressed in the state space. Moreover, if the state consists of position and velocity in the second order model case, the LQ method provides the optimal PD gains. In the case of $P_2(s)$ in (12), the state space model is expressed as

$$
\begin{bmatrix} \ddot{\theta} \\ \dot{\theta} \\ \theta_M \end{bmatrix} = \left[\begin{array}{cc|c} -\frac{C_M}{I_M} & -\frac{k}{I_M} & \frac{1}{I_M} \\ 1 & 0 & 0 \\ \hline 0 & 1 & 0 \end{array} \right] \begin{bmatrix} \dot{\theta} \\ \theta \\ \tau_M \end{bmatrix} \tag{13}
$$

where $\dot{\theta}$ and θ define the state, τ_M is the input, and θ_M is the output.
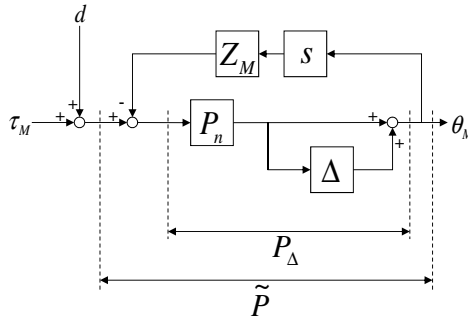

Fig. 14. Representation of actual actuator

The LQ performance index is

$$
J = \int_0^\infty \left[\theta_M^2(t) + R\tau_M^2(t) \right] dt = \int_0^\infty \left[\begin{bmatrix} \dot{\theta} \\ \theta \end{bmatrix}^T C^T C \begin{bmatrix} \dot{\theta} \\ \theta \end{bmatrix} + R\tau_M^2(t) \right] dt \tag{14}
$$

where R is the weighting factor to determine the relative importance between θ_M and τ_M. The control law for τ_M to minimize (14) is given by

$$
\tau_M(t) = -K \begin{bmatrix} \dot{\theta} \\ \theta \end{bmatrix}, \quad \text{where } K = R^{-1} B^T P \tag{15}
$$

In (15), P is the positive definite solution of the Riccati equation,

$$
0 = A^T P + PA - PBR^{-1}B^T P + C^T C \tag{16}
$$

where A, B, and C are as defined in (13). Since R is scalar, we have only one degree of freedom for designing the feedback controller. R should be sufficiently small to realize a high gain control law.

To analyze the performance of the closed loop system, the actuator model is reconfigured as shown in Fig. 14. It is assumed that the nominal plant P_n (i.e. P_2 in (12)) is subject to three undesired factors: the model variation Δ due to the interaction with a human, the unmodeled motor impedance Z_M (e.g. friction force), and the exogenous disturbance d. Since the resistive force due to the motor impedance is related to the velocity, a differential operator, s, appears in front of Z_M in Fig. 14. The perturbed system is expressed as

$$\tilde{P}(s) = \frac{P_\Delta(s)}{1 + sZ_M(s)P_\Delta(s)} \tag{17}$$

where

$$P_\Delta(s) = P_n(s)[1 + \Delta(s)] \tag{18}$$

Applying the feedback controller, $C(s)$, the perturbed closed loop control system in Fig. 11 is expressed as

$$E(s) = \left[\frac{\alpha(s)\tilde{P}(s)C(s)}{1 + \alpha(s)\tilde{P}(s)C(s)} \right] E_D(s) + \left[\frac{\alpha(s)\tilde{P}(s)}{1 + \alpha(s)\tilde{P}(s)C(s)} \right] d(s) \tag{19}$$

where $E_D(s)$ is the desired spring deflection. Note that the model variation is attenuated when control gains in $C(s)$ increases as long as the closed loop system remains asymptotically stable. As $|C(j\omega)| \to \infty$, $E(j\omega)$ is asymptotic to $E_D(j\omega)$ and is not influenced by $d(j\omega)$.

4.3   Robustness Enhancement

Since the PD control gains may be increased only in a limited range due to practical problems such as noise and instability caused by discretization, a better robust control method may be required to achieve the desired performance objectives. It is desirable to make the magnitude of the closed loop frequency response close to one over a sufficiently large frequency range.

The bandwidth of the human joint is about $4 \sim 8Hz$ [26] and the frequency response should be flat at least over this frequency range. Note that the closed loop transfer function significantly depends on $\alpha(s)$, which makes the dynamic transient vary significantly. In order to overcome this problem, the DOB (Disturbance Observer) may be introduced as shown in Fig. 15.
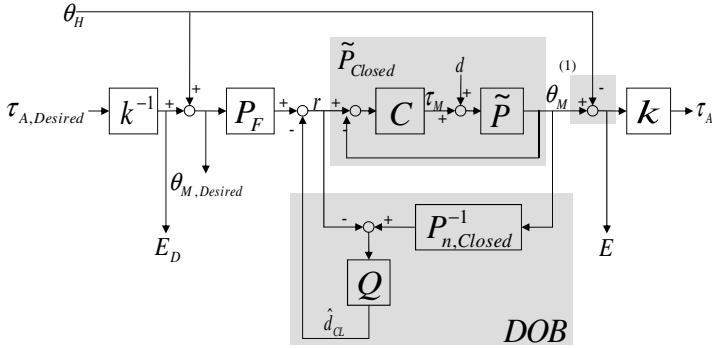
Fig. 15. Block diagram of the overall joint control system: The overall control method corresponds to Impedance Compensator in Fig. 1.

In general, the DOB may be used to:

1. estimate and cancel disturbance, and
2. compensate for the variation of plant dynamics by treating the variation as an equivalent disturbance.

In this application, the DOB is used more to the second objective although the disturbance cancellation is taking place also. For the basic properties of DOB, see [27].

It should be noted that the DOB is applied for the motor part only, i.e. the human joint angle is not fed into the DOB as shown in Fig. 15. Since the DOB is capable of rejecting exogenous disturbances, it increases the motor impedance significantly. Moreover, if E is fed back into the DOB, the human joint motion θ_H may be regarded as a disturbance [see (1) in Fig. 15] and rejected (or resisted) by the DOB. Since this is undesirable for human-robot interaction, the human joint angle should not be fed into the DOB.

The overall control scheme in Fig. 15 is as follows:

1. First, the desired spring deflection (E_D) is obtained from (3) on-line. Adding the human joint angle (θ_H) the desired position of the motor ($\theta_{M,Desired}$) is obtained as in (4). Note that if the desired torque is zero, then $\theta_{M,Desired}$ is the same as θ_H.
2. Second, the feedforward filter (P_F) is applied for compensation of the closed loop dynamics. P_F is designed based on the nominal closed loop model. In fact, the tracking performance of the motor is significantly improved by this feedforward filter.
3. Third, the PD controller (C in Fig. 15) is applied to attenuate the model variation. It allows increasing the bandwidth of DOB so that the performance of the overall system is improved significantly. The PD control gains are optimally obtained from (15) and (16) based on the nominal model in (12).
4. Finally, the DOB compensates for model variations resulted from human-robot interaction, and rejects undesired disturbances such as the friction

force. It makes the motor behave as the nominal model. Therefore, the feed-forward filter (P_F) remains effective.

It is assumed that the closed loop transfer function, $\tilde{P}_{Closed}(s)$, in Fig. 15 is expressed as

$$\tilde{P}_{Closed}(s) = P_{n,Closed}(s)\left[1 + \Delta_{Closed}(s)\right] \tag{20}$$

where $P_{n,Closed}(s)$ is the nominal closed loop dynamics obtained from $P_2(s)$ in (12) under PD control, i.e.

$$P_{n,Closed}(s) = \frac{P_2(s)C(s)}{1 + P_2(s)C(s)} \tag{21}$$

and $\Delta_{Closed}(s)$ is

$$\Delta_{Closed}(s) = \frac{(1 - \alpha(s))k}{I_M s^2 + C_M s + \alpha(s)k + C(s)} \tag{22}$$

Note that the closed loop transfer function in (21) is used as a nominal model in the design of DOB.

In the design of DOB, the selection of the filter labeled Q in Fig. 15 is important. The first requirement is that the order of $Q(s)$ must be such that $Q(s)P_{2,Closed}^{-1}(s)$ is realizable. The remaining two conditions ((23) and (24) below) make the closed loop system with DOB robust in terms of performance and stability. Namely, the DOB is effective at frequencies where

$$|Q(j\omega)| \approx 1 \tag{23}$$

The stability condition introduces another constraint, i.e.

$$|Q(j\omega)| < |\Delta_{Closed}(j\omega)|^{-1} \tag{24}$$

Notice that (23) and (24) require the magnitude of the model uncertainty to be less than one over a sufficiently large frequency range. Since the magnitude of the model uncertainty in (22) decreases as the PD control gains increase, the Q filter can be designed to have a sufficiently large bandwidth.

Even though the proposed controller stably controls the RSEA for every possible model in Fig. 9, a question arises that drastic changes of dynamic characteristics may introduce instability to the system. However, since phases of a human motion change smoothly and continuously [28] in normal conditions, the dynamic characteristics also change smoothly and continuously. When the dynamic model drastically changes (e.g., falling), however, stability may become a critical issue. In fact, simulations did not suggest such a stability problem even in the extreme cases.

The feedforward filter, P_F, may be determined by applying the pole-zero cancellation method, i.e.

$$P_F(s) = P_{n,Closed}^{-1}(s)P^*(s) \tag{25}$$

where $P_{n,Closed}(s)$ is as defined in (21). Since the inverse of the transfer function is usually unrealizable, $P^*(s)$ has been introduced to make the feedforward filter realizable. Also the magnitude of $P^*(j\omega)$ should be close to one over a sufficiently large frequency range. Note that the functions of $P^*(s)$ are the same as those of $Q(s)$ in DOB. For the simple design of the controllers, it is assumed that $P^*(s) = Q(s)$.

Arranging (18), (21), and (25) based on the control structure in Fig. 15, we obtain the transfer function of the motor part as follows

$$\theta_M(s) = \frac{Q(s)a(s)}{a(s)Q(s) + b(s)[1 - Q(S)]} \left[\theta_H(s) + \frac{\tau_{A,Desired}}{k}\right]$$
$$+ \frac{b(s)[1 - Q(s)]}{a(s)Q(s) + b(s)[1 - Q(s)]} \frac{\tilde{P}(s)}{1 + \tilde{P}(s)C(s)} d(s) \qquad (26)$$

where

$$a(s) = \frac{\tilde{P}(s)}{P_n(s)}, \; b(s) = \frac{1 + \tilde{P}(s)C(s)}{1 + P_n(s)C(s)} \qquad (27)$$

By applying (3) to (26), the transfer function of the overall system is obtained as follows

$$\tau_A(s) = k\left[\theta_M(s) - \theta_H(s)\right]$$
$$= Z_H(s)\theta_H(s) + Z_r(s)\tau_{A,Desired}(s) + Z_d(s)d(s) \qquad (28)$$

where

$$Z_H(s) = k\left[\frac{a(s)Q(s)}{a(s)Q(S) + b(s)[1 - Q(s)]} - 1\right] \qquad (29)$$

$$Z_r(s) = \frac{a(s)Q(s)}{a(s)Q(s) + b(S)[1 - Q(s)]} \qquad (30)$$

$$Z_d(s) = k\frac{b(s)[1 - Q(s)]}{a(s)Q(s) + b(S)[1 - Q(s)]} \frac{\tilde{P}(s)}{1 + \tilde{P}(s)C(s)} \qquad (31)$$

$Z_H(s)$, $Z_\tau(s)$, and $Z_d(s)$ represent transfer functions to the torque output from the human joint angle $\theta_H(s)$, the desired output $\tau_{A,Desired}(s)$ and the exogenous disturbance input $d(s)$, respectively. According to the performance objectives, it is ideal to have $Z_H(s) = 0$, $Z_\tau(s) = 1$, and $Z_d(s) = 0$, which are not possible due to stability among other reasons. Note that when $Q(s)$ is close to one, (29),(30), and (31) are asymptotic to

$$Z_H(s) \approx 0, \; Z_r(s) \approx 1, Z_d(s) \approx 0 \qquad (32)$$

$Z_H(s) \approx 0$ implies that the RSEA does not generate any resistive torque to the human joint motion, i.e. motor impedance is decreased. $Z_\tau(s) \approx 1$ represents that the actuator generates the torque as desired precisely. Finally, $Z_d(s) \approx 0$ means that the exogenous disturbance does not affect the torque output.

4.4 Reformulation into Force Feedback Loop

Since the spring plays a role of a torque sensor as well as an energy buffer, it may be reasonable to control the RSEA by feeding back the torque estimated from the spring deflection. The proposed control system in Fig. 15 also can be represented in the force feedback configuration. The control law in by Fig. 15 implies

$$\tau_M(s) = C(s)\left[\frac{P_{n,Closed}^{-1}(s)Q(s)}{k(1-Q(s))}(\tau_{A,Desired} - \tau_A) - \frac{\tau_A}{k} - \theta_H\right] \quad (33)$$

where $P_{n,Closed}(s)$, $Q(s)$, $C(s)$, θ_H are as defined above. τ_A and $\tau_{A,Desired}$ are the estimated and the desired torques, respectively.
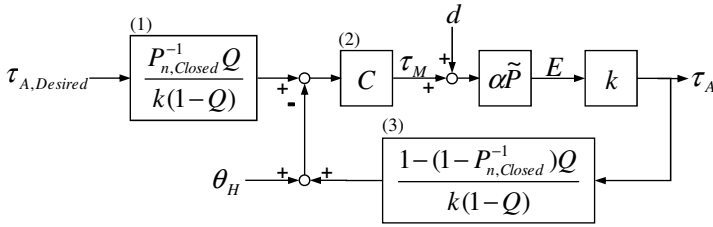

Fig. 16. Block diagram of the controllers in Fig. 15 reformulated into a simple feedback loop: k is a spring constant, and α and $\tilde{P}$ are as defined in (6) and (18), respectively.

Equation (33) is realized in a block diagram shown in Fig. 16. Noting (8) and Fig. 14, $\tau_A = k\alpha\tilde{P}(\tau_M + d)$, which means that the control system shown in Fig. 16 is equivalent to that in Fig. 15. Note that the new block diagram includes a feedforward filter ((1) in the figure) and feedback controllers ((2) and (3) in the figure). The generated torque τ_A is estimated by multiplying k to the spring deflection E. It also should be noted that the human joint angle, θ_H, is included in the feedback loop. This is not shown in the fundamental force feedback systems shown in Fig. 11. It acts as a feedforward signal such that the control system considers the human motion. The controllers in Fig. 16 do not include human factors (e.g., physical properties of body segments, etc.) and are designed based on the nominal model of the motor part. Therefore, the proposed control system can be applied to human-robot interaction applications for different people without measuring the properties of body segments.

5   Performance Analysis by Experiments

Once a RSEA is stabilized by applying the overall control system in Fig. 15, it is desired to verify the following performance objectives by experiments:

1. Capability of rejecting the undesired disturbances including the rotor inertia and any disturbances, i.e., the controlled RSEA should exhibit low impedance,
2. Capability of generating the desired torque precisely, and
3. Capability of generating the desired torque with a sufficient frequency bandwidth.

5.1 Experimental Setup

A RSEA shown in Fig. 5 was used to verify the proposed systems. For the design of the controllers, the nominal model of the motor should be obtained first, i.e. I_M and C_M are to be identified. Note that the spring constant, k, is known as shown in Table. 1. The motor used in the RSEA is an EC-powermax30 motor of Maxon Motor Company. The reduction ratio is 113:1 and the maximum power of the motor is $200W$. The system model obtained by sinusoidal excitations is

$$P(s) = \frac{4.463}{s^2 + 9.821s + 22.31} \tag{34}$$

The model in (34) includes a torque constant of the servo amplifier.

The PD controller, $C(s)$, was designed by the LQ method as discussed. R in (14) was set to 0.0001. $P_{n,Closed}(s)$ was obtained by (21) with the designed $C(s)$ and $P(s)$. The Q filter in DOB was a lowpass filter with the cut-off frequency of $20Hz$. Since the frequency range of the human motion is about $4 \sim 8Hz$, $20Hz$ is enough for the frequency bandwidth of actuation. Since $P_{n,Closed}(s)$, $C(s)$, $Q(s)$, and k are known, the control law in (33) is realizable.

5.2 Motor Impedance Test

As mentioned already, actuators for human-robot interaction should have low mechanical impedance. Otherwise, human has to make an additional effort to overcome the resistive forces. Fig. 17 shows the relation between the actual resistive torques and the angular velocities under the proposed control system when the desired torque output was zero. To exert the precise angular velocity to the RSEA from the load side, i.e. the human joint in case of assistive device applications, an additional motor, which has large mechanical impedance, was used. For comparison of the performance, the figure also shows the results under PD control (i.e. $C(s)$ without DOB) and open loop control. By applying the proposed control system, the measured torque was close to zero [see "Proposed Control" line in Fig. 17], which means no resistive torque is generated regardless of motion of the rotor. For more quantitative comparison, the curve fits were obtained (continuous lines in the figure) with the following fitting function,

$$f(\omega) = a_1 + a_2\mathrm{sgn}(\omega) + a_3\omega \tag{35}$$

where a_1, a_2, and a_3 represent terms due to bias, nonlinear friction, and linear damping, respectively. For the desired performance, i.e. to have low motor

impedance, all parameters in (35) should be zero. Table. 3 shows the obtained parameters for each control method. Note that the magnitude of each parameter significantly decreases under the proposed control system. For example, the magnitudes of the bias, the friction, and the linear damping forces are decreased by 99.13%, 99.85%, and 99.79% from the open loop performance, respectively. Comparing with the PD control, they are reduced by 86.2%, 85.9%, and 98.18%, respectively. Note that the proposed controller effectively reduces the linear damping effects, which means the proposed one shows a good performance over the enough frequency bandwidth.

Table 3. Coefficients of motor impedance

Control Method	a_1 Bias[3]	a_2 Friction[4]	a_3 Linear Damping[5]
No Control	-1.509×10^0	9.572×10^{-1}	1.414×10^{-1}
PD Control[1]	-9.534×10^{-2}	1.040×10^{-1}	1.614×10^{-2}
Proposed Control[2]	1.311×10^{-2}	1.464×10^{-3}	-2.941×10^{-4}

Each number shows the coefficient obtained by the curve fit based on (31).
[1,2] See block diagrams in Fig. 11 and Fig. 15, respectively.
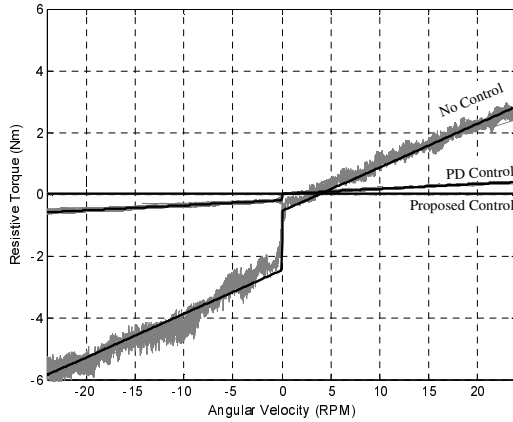[3,4,5] use the units of $[Nm]$, $[Nm]$ and $[Nm/(rad/s)]$, respectively.

Fig. 17. Motor impedance test about angular velocity: the desired torque is zero

Fig. 18 shows the relation between the generated torques and the desired torques under the proposed control method when the angular velocity was fixed
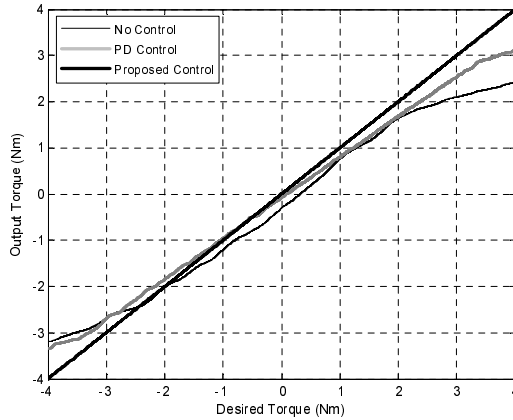
Fig. 18. Linearity test about control input: the angular velocity of rotor is fixed to zero
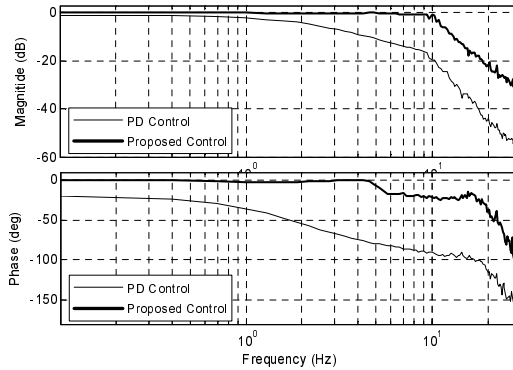

Fig. 19. Frequency response of each control scheme

to zero, i.e. the frame ((c) in Fig. 5) was fixed mechanically. This setup is as defined in *Case 2* in Fig. 9. Fig. 18 verifies that a RSEA controlled by the proposed control system generates torques as desired precisely. The output torque was estimated by multiplying the spring constant to the deflection. In the linear-region shown in Fig. 7, the torque estimation is reliable. Applying the proposed control system, the nonlinearities were compensated.

5.3   Frequency Response Analysis

It is also required that the RSEA generates the desired torque over a sufficiently large frequency range. Fig. 19 shows the frequency responses of the RSEA controlled by the proposed controller. The experimental setup for frequency response analysis was the same as in Fig. 17 except for a mass attached to the

load side of the RSEA. Otherwise, the output velocity of the RSEA easily saturates to the maximum, which implies that the inertia of the RSEA is eliminated effectively. This setup may correspond to *Case 1* in Fig. 9. It is known that the human motion contains frequency components up to $4 \sim 8Hz$ [26]. Note that the RSEA with the proposed control algorithm generates the desired torque properly up to about $10Hz$.

5.4   Verification by Human Walking Experiments

Experiments shown in Figs. 17, 18, and 19 verified the performances of RSEA without human factors. Therefore, they did not verify if the proposed control system robustly rejects the undesired disturbances and reduces the actuator impedance in the environments interacting with a human. To verify the robustness of the control system, RSEAs were installed at an active orthosis system as shown in Fig. 20. Two actuators were attached to each knee and ankle joint and controlled by the proposed control algorithm without change of parameters. The human factors of the knee and ankle joints (e.g. the inertia and the damping coefficient) are different so that the robustness may be verified if both actuators show the same performances.

Setting the desired torque to zero, a subject wearing the active orthosis was walking on a treadmill as shown in Fig. 20(b). It is desired that the subject does not feel any resistance from the actuators. Fig. 21 shows the ankle joint motion and the torque generated by the RSEA. As shown in Fig. 21(a), the motor followed the human joint motion to keep zero spring deflection. However, it was delayed by a few samples due to the phase delay of $P^*(s)$ in the feedforward filter
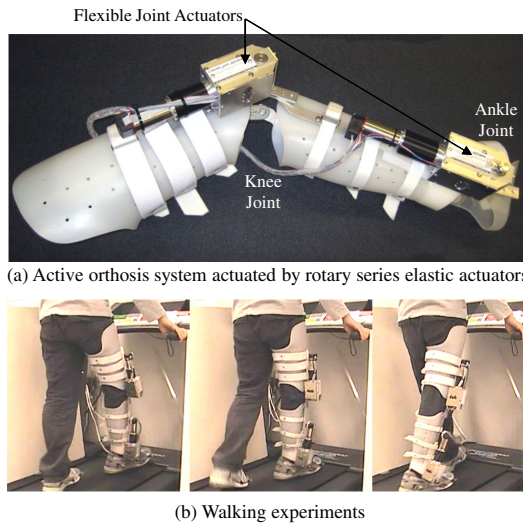

(a) Active orthosis system actuated by rotary series elastic actuators

(b) Walking experiments

Fig. 20. Application of rotary series elastic actuator

[see (25)]. In this experiment, $P^*(s)$ was the same as the Q filter in DOB for the simple design of controllers. If the cut-off frequency of $P^*(s)$ is increased, the resistive torque shown in Fig. 21(b) is decreased significantly, but a human feels a high frequency vibration, which makes the human uncomfortable. Therefore, the filter should be selected considering the human comfort as well as the control performance. Even though the resistive torque was generated due to the time delay, the magnitude of the resistive torque was small ($4.25 \times 10^{-6} Nm$ in root-mean-square, $9.44 \times 10^{-2} Nm$ in peak-to-peak) so that the subject did not feel any resistance. The resistive torque was calculated from the spring deflection measured by encoders.
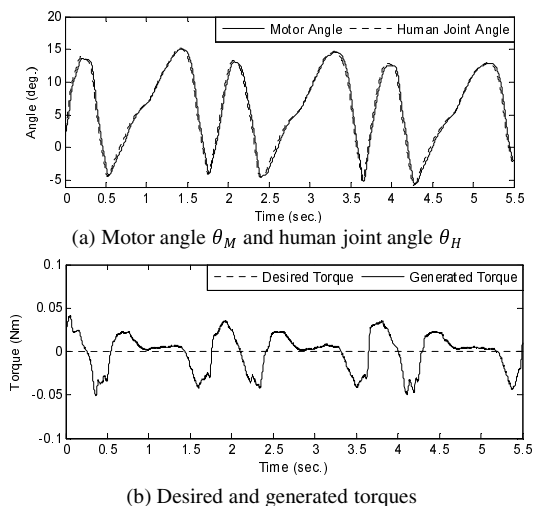

(a) Motor angle θ_M and human joint angle θ_H

(b) Desired and generated torques

Fig. 21. Experimental data on ankle joint during walking: the desired assistive torque was zero

It is also desired that the RSEA installed at the knee joint shows the same performance without changing the control parameters. Fig. 22 shows data on the knee joint during the same experiment. Similarly, the motor followed the human joint motion with a time delay of a few samples as shown in Fig. 22(a). Since the maximum angular velocity of the knee joint was greater than that of the ankle joint, the resistive torque of the knee actuator was larger. Fig. 22(b) shows the resistive torque generated by the actuator. The resistive torque is large at high angular velocities (e.g. see about 0.9 seconds). The generated resistive torque was $3.33 \times 10^{-4} Nm$ in root-mean-square and $1.49 \times 10^{-1} Nm$ in peak-to-peak. Even though the magnitude of the resistive torque is slightly increased compared with the ankle joint, the RSEA showed the similar performance for a different joint without changing the control parameters. The increased resistive torque may be because of relatively higher angular velocity of knee joint motions while the control performance can be affected by the human motions (i.e. $Z_H(s)$ in
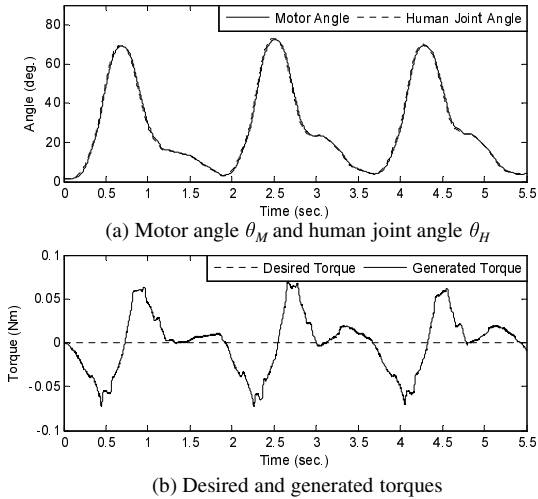
(a) Motor angle θ_M and human joint angle θ_H

(b) Desired and generated torques

Fig. 22. Experimental data on knee joint during walking: the desired assistive torque was zero

(29) is not zero in reality). However, it should be noted that the stability was not affected by the human motions or the different human factors. Therefore, the experiment in Fig. 22 verified that the proposed method can be applied to systems that physically interact with a human without considering the human factors.

An experiment in Fig. 23 was performed to check if the RESA with the proposed control algorithm generates the desired torque precisely. In the actual cases, the desired torque should be determined for particular purposes, e.g. rehabilitation or human power augmentation. Since this chapter focuses on how to control an actuator for the force mode actuation, the desired torque was simply set as a sinusoidal wave as shown in Fig. 23(b). For examples of the higher level control algorithms that determine the desired torque, see [3], [6], [9]-[11]. The subject was resisting the generated torque for the first 11 seconds and started the walking motion. Note that the human joint motion shown in Fig. 23(a) is slightly different for each stride because the human motion was affected by the generated torque. Fig. 23(a) also shows the motor angle as well as the knee joint angle. The motor followed the human joint motion with a certain offset such that the spring has a proper deflection. Since the motor angle was precisely controlled to have the desired spring deflection, the generated torque matched the desired torque, as shown in Fig. 23(b). The magnitude of the torque error shown in Fig. 23(c) was slightly increased when the human motion was active but the system was still stable and generated the desired torque successfully.
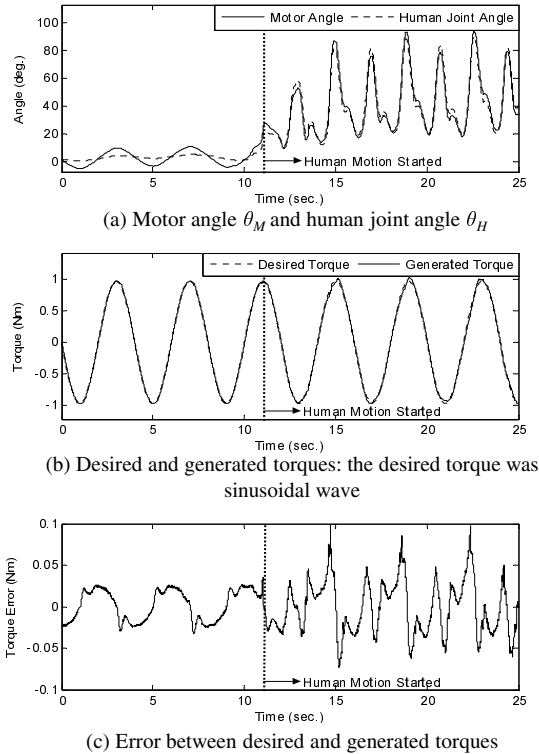
(a) Motor angle θ_M and human joint angle θ_H

(b) Desired and generated torques: the desired torque was sinusoidal wave

(c) Error between desired and generated torques

Fig. 23. Experimental data on knee joint when the desired torque varies

6   Conclusions

In applications involving human-robot interaction, actuators should have zero impedance for precise force control. In spite of numerous efforts, the actuator design is still one of the most evident problems in this field. In this chapter, a rotary series elastic actuator (RSEA) was designed and its control method was proposed for improved human-robot interaction.

In the RSEA, a torsional spring was installed between a human joint and a motor as the energy buffer. By controlling the motor part with a position control method, the torque was precisely generated via the spring deflection.

The use of spring introduced challenges to the design of controllers. In this chapter, the optimal PD control, the feedforward control, and the disturbance observer were applied to robustly control the RSEA under the environments interacting with a human. It was shown that the proposed control method meets the desired performances: the RSEA precisely generated the torque as desired, and its impedance has been decreased significantly. In this chapter, the performance was verified by experiments.

The RSEA and its control algorithm proposed in this chapter may provide a good solution for actuation methods in applications of human-robot interaction, in particular wearable robots. Since the control method does not require any physical properties of the human body, it is unnecessary to design the controllers for each individual. It allows precise force (or torque) mode control, and it provides the foundation to the design of higher level controls for human-robot interaction.

Series elastic actuators, including RSEA, provide both advantages and disadvantages for human assistive robots. The reduced mechanical impedance and improved torque precision make the robots able to assist people with light impairments including the elderly and patients with progressive muscular weakness. Most of the target users of the assistive robots are such people, and thus the series elastic actuators can contribute to realization of an effective assistive robot for a number of potential users. However, due to the use of additional mechanical peripherals, such as a spring, the power density, i.e., the power-to-weight ratio, becomes low. This is a clear disadvantage of the series elastic actuators for application to mobile systems. These factors should be considered in selection of an actuation system for assistive robots.

References

1. Hayashi, T., Kawamoto, H., Sankai, Y.: Control method of robot suit HAL working as operator's muscle using biological and dynamical information. In: Proc. IEEE/RSJ Int. Conf. Intell. Robots Syst.: IROS 2005, pp. 3063–3068 (2005)
2. HAL-5, Cyberdyne Co., `http://www.cyberdyne.jp`
3. Kazerooni, H., Racine, J., Huang, L., Steger, R.: On the control of the berkeley lower extremity exoskeleton (BLEEX). In: Proc. IEEE Int. Conf. Robotics Autom.: ICRA 2005, pp. 4353–4360 (2005)
4. Zoss, Kazerooni, H., Chu, A.: Biomechanical design of the berkeley lower extremity exoskeleton (BLEEX). IEEE/ASME Trans. Mechatronics 11(2), 128–138 (2006)
5. Yamamoto, K., Ishii, M., Noborisaka, H., Hyodo, K.: Stand alone wearable power assisting suit-sensing and control systems. In: Proc. IEEE Int. Workshop Robot Human Interactive Commun.: ROMAN 2004, pp. 661–666.
6. Kong, K., Jeon, D.: Design and control of an exoskeleton for the elderly and patients. IEEE/ASME Trans. Mechatronics 11(4), 428–432 (2006)
7. Kong, K., Jeon, D.: Fuzzy control of a new tendon-driven exoskeletal power assistive device. In: Proc. IEEE/ASME Int. Conf. Adv. Intell. Mech.: AIM 2005, pp. 146–151 (2005)
8. Banala, S.K., Agrawal, S.K., Fattah, A., Krishnamoorthy, V., Hsu, W., Scholz, J., Rudolph, K.: Gravity-balancing leg orthosis and its performance evaluation. IEEE Trans. Robotics 22(6), 1228–1239 (2006)
9. Riener, R., Lünenburger, L., Jezernik, S., Anderschitz, M., Colombo, G., Dietz, V.: Patient-cooperative strategies for robot-aided treadmill training: first experimental results. IEEE Trans. Neural Syst. Rehabil. Eng. 13(3), 380–394 (2005)
10. Hogan, N.: Impedance control: an approach to manipulation, parts I, II, III. J. Dyn. Syst., Meas. Control 107, 1–23 (1985)

11. Blaya, J., Herr, H.: Adaptive control of a variable-impedance ankle-foot orthosis to assist drop-foot gait. IEEE Trans. Rehabil. Eng. 12(1), 24–31 (2004)
12. Bar-Cohen, Y.: Electroactive Polymer (EAP) Actuators as Artificial Muscles - Reality, Potential and Challenges. SPIE Press (2004)
13. Noritsugu, T., Tanaka, T.: Application of rubber artificial muscle manipulator as a rehabilitation robot. IEEE/ASME Trans. Mechatronics 2(4), 259–267 (1997)
14. Buerger, S.P., Hogan, N.: Complementary stability and loop shaping for improved human-robot interaction. IEEE Trans. Robotics 23(2), 232–244 (2007)
15. Paluska, D., Herr, H.: Series elasticity and actuator power output. In: Proc. IEEE Int. Conf. Robotics Autom.: ICRA 2006, pp. 1830–1833 (2006)
16. Kong, K., Tomizuka, M.: Flexible joint actuator for patient's rehabilitation device. In: Proc. IEEE Int. Symp. Robot Human Interactive Commun.: ROMAN 2007, pp. 1179–1184 (2007)
17. Pratt, J., Krupp, B., Morse, C.: Series elastic actuators for high fidelity force control. Int. J. Ind. Robot 29(3), 234–241 (2002)
18. Low, K.H.: Initial experiments of a leg mechanism with a flexible geared joint and footpad. Adv. Robotics 19(4), 373–399 (2005)
19. Pratt, G.A., Williamson, M.W.: Series elastic actuators. In: Proc. IEEE/RSJ Int. Conf. Intell. Robotics Syst.: IROS, Pittsburgh, PA, pp. 399–406 (1995)
20. Robinson, D.W., Pratt, J.E., Paluska, D.J., Pratt, G.A.: Series elastic actuator development for a biomimetic walking robot. In: Proc. IEEE/ASME Int. Conf. Adv. Intell. Mech.: AIM 1999, Atlanta, GA, pp. 561–568 (1999)
21. Williamson, M.M.: Series Elastic Actuators. M.S. Thesis, Massachusetts Institute of Technology (June 1995)
22. Alter, D.M., Tsao, T.C.: Dynamic stiffness enhancement of direct linear motor feed drives for machining. In: Proc. American Cont. Conf.: ACC 1994, vol. 3, pp. 3303–3307 (1994)
23. Katsura, S., Matsumoto, Y., Ohnishi, K.: Analysis and experimental validation of force bandwidth for force control. IEEE Trans. Ind. Electronics 53(3), 922–928 (2006)
24. McKnight, E.: Control of Joint Forces: a New Perspective. Afcea International Press (1989)
25. Shigley, J., Mischke, C., Budynas, R.: Mechanical Engineering Design, ch. 10. McGraw-Hill (2004)
26. Winter, D.: Biomechanical Motor Control and Human Movement. Wiley-Interscience Publication (1990)
27. Lee, H., Tomizuka, M.: Robust motion controller design for high-accuracy positioning systems. IEEE Trans. Ind. Electronics 43(1), 48–55 (1996)
28. Kong, K., Tomizuka, M.: Smooth and continuous human gait phase detection based on foot pressure patterns. In: Proc. IEEE Int. Conf. Robotics Autom.: ICRA 2008, pp. 3678–3683 (2008)
29. Masia, L., Krebs, H., Cappa, P., Hogan, N.: Design and characterization of hand module for whole-arm rehabilitation following stroke. IEEE/ASME Trans. Mechatronics 12(4), 399–407 (2007)